Enhancements and applications of induced aberration theory

Crowther, Blake, Sasián, José, Hoffman, Jeffrey

Blake G. Crowther, José Sasián, Jeffrey M. Hoffman, "Enhancements and applications of induced aberration theory," Proc. SPIE 11479, Roland V. Shack Memorial Session: A Celebration of One of the Great Teachers of Optical Aberration Theory, 114790F (21 August 2020); doi: 10.1117/12.2569041

SPIE.

Event: SPIE Optical Engineering + Applications, 2020, Online Only

Enhancements and Applications of Induced Aberration Theory

Blake G. Crowther*[a], José Sasián**[b], Jeffrey M. Hoffman***[a]
[a]Synopsys, Optical Solutions Group, 199 S. Los Robles Ave., Pasadena CA 91101; [b]Wyant College of Optical Sciences, The University of Arizona, 1630 E. University Blvd., Tucson, AZ 85721

ABSTRACT

Intrinsic and induced aberrations can be important contributors to the total aberration content of a lens. Theory for induced aberrations has been explored and recently advanced. Macros for calculating and targeting intrinsic and induced aberrations have been written. We briefly discuss wave aberration theory and induced aberration theory, including algorithmic advancements. We demonstrate the application of the recent theory and new macros in lens optimization.

Keywords: Roland Shack, intrinsic aberrations, induced aberrations, extrinsic aberrations, optimization

1. INTRODUCTION

The description of aberration terms has taken various forms over the years. The wave theory of aberrations as pioneered by H. H. Hopkins at Imperial College in London, England introduced a unique perspective on aberration theory [1]. That perspective was extended by R. V. Shack, who studied under Hopkins, and taught to students at the Optical Sciences Center, now the Wyant College of Optical Sciences in Tucson, Arizona [2], [3]. We, the authors of this paper, learned the Shack version of aberration theory. That theory, and extensions of it, can be applied to optical design in many different ways. We have optimized systems using this theory and show an interesting application example in this paper. It is our hope that others can more readily use the theory and optimization capability shown to further their own optical designs.

1.1 Aberration Forms

The wave aberration theory as taught by Shack describes the wavefront departing the exit pupil of an optical system converging toward the ideal field point in the image plane. Aberrations are deviations of the actual wavefront from the perfect spherically converging wavefront, or reference sphere, measured in optical path units. The deviations or aberrations, for rotationally symmetric systems, are described using the following polynomial expansion in vector notation.

$$W(\vec{H},\vec{\rho}) = \sum_{j,m,n} W_{klm}(\vec{H}\cdot\vec{H})^{j}(\vec{H}\cdot\vec{\rho})^{m}(\vec{\rho}\cdot\vec{\rho})^{n}$$

The aberration function is $W(\vec{H},\vec{\rho})$, the individual aberration coefficients are $W_{k,l,m}$, the normalized field coordinate is $\vec{H}$, the normalized exit pupil coordinate is $\vec{\rho}$, $k=2j+m$, and $l=2n+m$ in the above equation. The equation can also be expressed in algebraic terms as follows.

$$W(\mathrm{H},\rho,\theta) = \sum_{j,m,n} W_{klm}H^{k}\rho^{l}\cos^{m}\theta$$

The angle between the field vector and exit pupil vector is θ in the above equation. Figure 1 shows a graphical depiction of the coordinate system and relevant terms.

* blakec@synopsys.com; https://www.synopsys.com/optical-solutions.html

** jose.sasian@optics.arizona.edu; www.optics.arizona.edu

*** jhoffman@synopsys.com; https://www.synopsys.com/optical-solutions.html

Roland V. Shack Memorial Session: A Celebration of One of the Great Teachers of Optical Aberration Theory, edited by John P. Lehan, Proc. of SPIE Vol. 11479, 114790F · © 2020 SPIE
CCC code: 0277-786X/20/$21 · doi: 10.1117/12.2569041

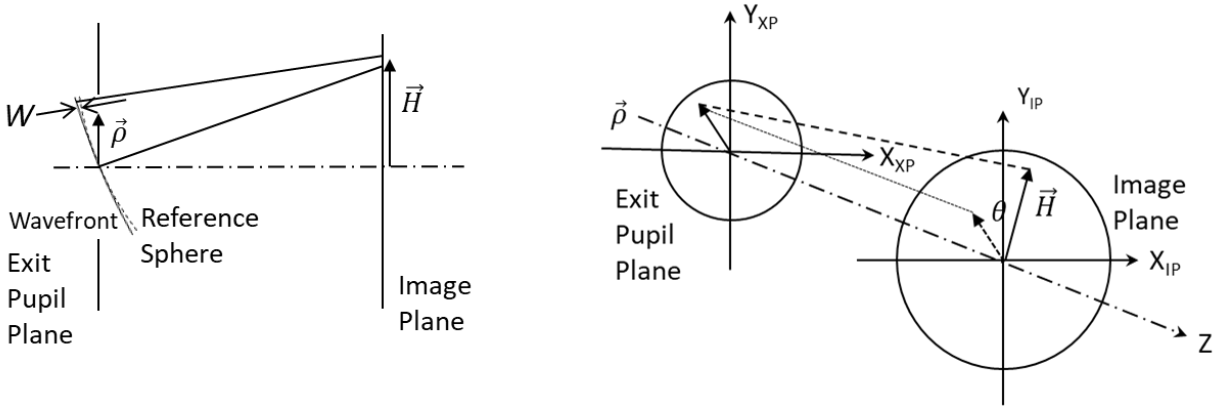

Figure 1. Coordinate system and variable depictions for describing aberrations using the Shack representation

Shack was fond of visualizing the aberration forms. He taught that in addition to calculating aberration coefficients, the ability to visualize them was helpful in developing intuition into the behavior of an optical system. A complete list of the aberration terms to sixth order can be seen in Sasián [4]. We list the aberration terms by family to sixth order as Shack did in Table 1 [3]. We have neglected the field coordinate or H in the figures since changes in H do not affect the form of the aberration at the pupil. The grid figures in Table 1 were a novelty when Shack introduced them to illustrate the wavefront deformation forms, i.e. the aberrations.

Aberrations can be further visualized by showing them in three-dimensional form using special eyeglasses with computer graphics, stereo eyeglass viewers with printed pages developed for visualizing three dimensional figures, or simply by "training" one's brain to see three-dimensionally while staring at stereo pairs, to paraphrase Shack [2]. We show selected stereo pairs in Figure 2 and Figure 3 to allow the reader to start such brain training. One way to generate other pairs is to print duplicate figures side-by-side separated by approximately the pupillary distance (~60 mm).

The reader will notice that our emphasis on aberration visualization is continued in all sections of this paper. Our experience shows that the ability to visualize aberrations or aberration quantities throughout an optical system can help one understand the behavior of the optical system and optimize its performance.

Table 1. Aberration forms and figures by family [2].

Spherical, $m = 0$	Coma, $m = 1$	Astigmatism, $m = 2$	$m = 3$
W_{k00} 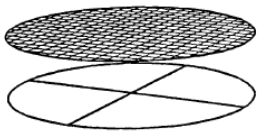			
W_{k20} 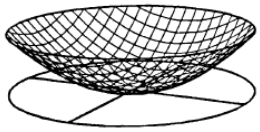	W_{k11} 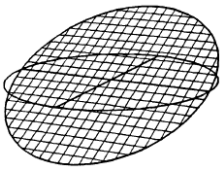		
W_{k40} 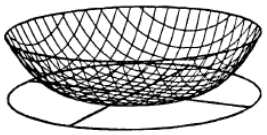	W_{k31} 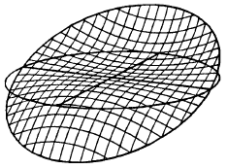	W_{k22} 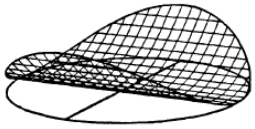	
W_{k60} 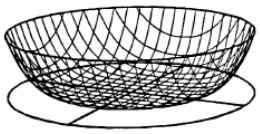	W_{k51} 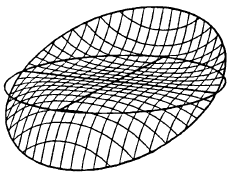	W_{k42} 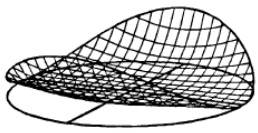	W_{k33} 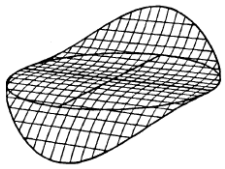

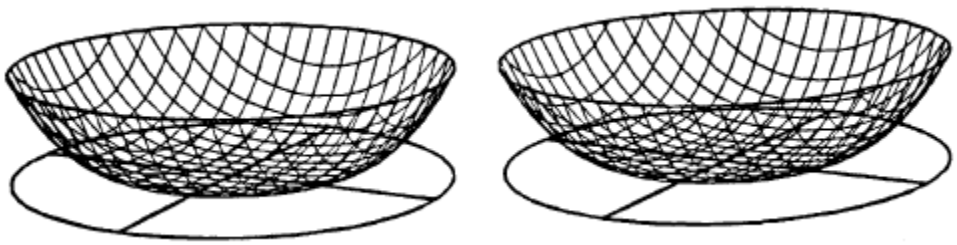

Figure 2. Stereo pair for spherical aberration, W_{040}

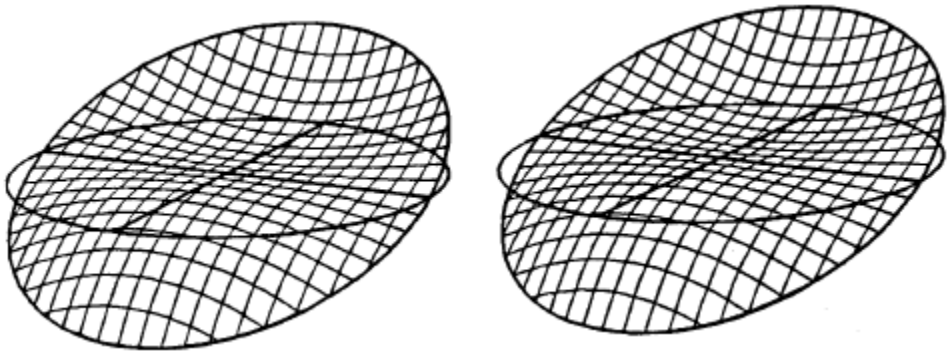

Figure 3. Stereo pair for coma, W_{131}

1.2 Intrinsic and Induced Aberrations

Early in the development of the theory of aberrations it was realized that the aberrations contributed by an optical component, whether it is a single surface or a system of surfaces, depends on the light beam aberration prior to that component. Thus, the aberration contributed by the component when there was no previous beam aberration was described as intrinsic aberration. When there was prior beam aberration, the additional aberration contributed by the component was called extrinsic, or induced aberration.

Induced aberration can be thought of as the synergy of the interaction between two components, A and B, when both individually contribute aberration. The total image aberration function $W(\vec{H},\vec{\rho})$ of the combination is not simply the sum of the intrinsic contributions of the two components, $W_A(\vec{H},\vec{\rho}) + W_B(\vec{H},\vec{\rho})$. There is an additional term $W_E(\vec{H},\vec{\rho})$ that represents the induced aberration; thus, the total aberration function of the combination is

$$W(\vec{H},\vec{\rho}) = W_A(\vec{H},\vec{\rho}) + W_B(\vec{H},\vec{\rho}) + W_E(\vec{H},\vec{\rho})$$

where $\vec{H}$ and $\vec{\rho}$ together specify any ray in the combined system and are defined in Section 1.1.

The induced aberration $W_E(\vec{H},\vec{\rho})$ comes about because the field vector and the aperture vector for the system may not be exactly the same as for the components. Thus, the total aberration can be also written as

$$W(\vec{H},\vec{\rho}) = W_A(\vec{H}_A,\vec{\rho}_A) + W_B(\vec{H}_B,\vec{\rho}_B)$$

However, the field vector for the system coincides with the field vector for component A, and the exit pupil vector of the system coincides with the exit pupil vector of component B, and so we can write

$$\vec{H}_A = \vec{H},\ \vec{H}_B = \vec{H} + \Delta\vec{H}_A,\ \vec{\rho}_B = \vec{\rho} \text{ and } \vec{\rho}_A = \vec{\rho} + \Delta\vec{\rho}_B,$$

where $\Delta\vec{H}_A$ and $\Delta\vec{\rho}_B$ are the transverse aberrations of the ray defined by $\vec{H}$ and $\vec{\rho}$ at the image plane of component A and at the entrance pupil of component B, respectively. In particular, we have

$$\Delta\vec{\rho}_B = -\frac{1}{\mathcal{K}}\vec{\nabla}_H \bar{W}_B(\vec{H},\vec{\rho}),$$

where $\vec{\nabla}_H \bar{W}_B(\vec{H},\vec{\rho})$ stands for the gradient with respect to $\vec{H}$ of the pupil aberration function of component B, and $\mathcal{K}$ is the system's Lagrange invariant.

The term $\Delta\vec{\rho}_B$ states that the entrance pupil of component B is distorted and does not match the undistorted exit pupil of component A. The fourth order pupil distortion is graphically shown in Figure 4.

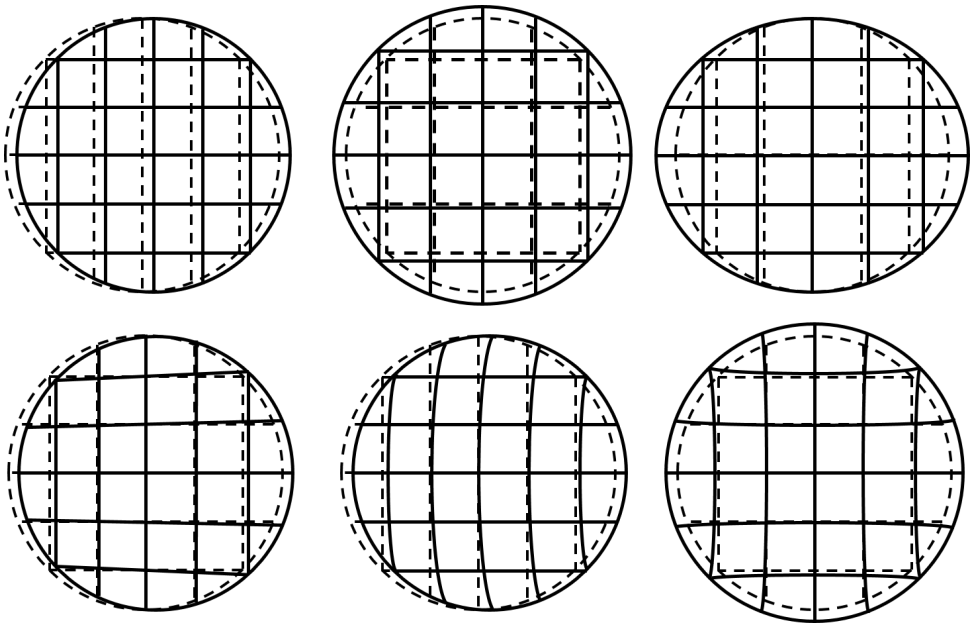

Figure 4. Fourth order pupil distortion aberrations of component B (solid line) versus the undistorted pupil of component A (dashed line).

Then the total image aberration function is

$$W(\vec{H},\vec{\rho}) = W_A(\vec{H},\vec{\rho}+\Delta\vec{\rho}_B) + W_B(\vec{H}+\Delta\vec{H}_A,\vec{\rho}).$$

Because the reference sphere that determines the wave aberration function is centered at the ideal image point for both components, A and B, we have that, to the sixth order of approximation in $\vec{H}$ and $\vec{\rho}$, the equality $W_B(\vec{H}+\Delta\vec{H}_A,\vec{\rho}) = W_B(\vec{H},\vec{\rho})$ holds. This is a significant and simplifying feature of the wave theory of aberrations. Thus, we have that the total aberration function for the system can be written to sixth order as

$$W(\vec{H},\vec{\rho}) = W_A(\vec{H},\vec{\rho}+\Delta\vec{\rho}_B) + W_B(\vec{H},\vec{\rho}).$$

Further, by adding and subtracting $W_A(\vec{H},\vec{\rho})$, and using $\Delta\vec{\rho}_B = -\frac{1}{\mathcal{K}}\vec{\nabla}_H\bar{W}_B(\vec{H},\vec{\rho})$, we can finally write

$$W(\vec{H},\vec{\rho}) = W_A(\vec{H},\vec{\rho}) + W_B(\vec{H},\vec{\rho}) - \frac{1}{\mathcal{K}}\vec{\nabla}_H\bar{W}_B(\vec{H},\vec{\rho})\cdot\vec{\nabla}_\rho W_A(\vec{H},\vec{\rho}),$$

that states, that to the sixth order of approximation, the image aberration function of the combination of two components A and B is the sum of the intrinsic contributions plus an induced term $-\frac{1}{\mathcal{K}}\vec{\nabla}_H\bar{W}_B(\vec{H},\vec{\rho})\cdot\vec{\nabla}_\rho W_A(\vec{H},\vec{\rho})$, which is the dot product of the transverse ray image aberrations of component A and the pupil transverse ray aberrations of component B.

Since the image and pupil aberration functions have no second order terms, there are no fourth order induced terms. However, there are fourth order image and pupil aberrations which result in the sixth order induced aberrations given in Table 2.

Table 2. Induced aberration coefficients from combining component A and component B

$W_{060E} = -\frac{1}{\mathcal{K}}(4W_{040}^{A}\bar{W}_{311}^{B})$	$W_{331E} = -\frac{1}{\mathcal{K}}\begin{pmatrix}5W_{131}^{A}\bar{W}_{131}^{B} + 4W_{220}^{A}\bar{W}_{220}^{B} \\ +4W_{220}^{A}\bar{W}_{222}^{B} + 4W_{222}^{A}\bar{W}_{220}^{B} \\ +W_{311}^{A}\bar{W}_{311}^{B} + 16W_{040}^{A}\bar{W}_{040}^{B}\end{pmatrix}$
$W_{151E} = -\frac{1}{\mathcal{K}}\begin{pmatrix}3W_{131}^{A}\bar{W}_{311}^{B} + 8W_{040}^{A}\bar{W}_{220}^{B} \\ +8W_{040}^{A}\bar{W}_{222}^{B}\end{pmatrix}$	$W_{422E} = -\frac{1}{\mathcal{K}}\begin{pmatrix}2W_{311}^{A}\bar{W}_{222}^{B} + 4W_{220}^{A}\bar{W}_{131}^{B} \\ +6W_{222}^{A}\bar{W}_{131}^{B} + 8W_{131}^{A}\bar{W}_{040}^{B}\end{pmatrix}$
$W_{242E} = -\frac{1}{\mathcal{K}}\begin{pmatrix}2W_{222}^{A}\bar{W}_{311}^{B} + 4W_{131}^{A}\bar{W}_{220}^{B} \\ +6W_{131}^{A}\bar{W}_{222}^{B} + 8W_{040}^{A}\bar{W}_{131}^{B}\end{pmatrix}$	$W_{420E} = -\frac{1}{\mathcal{K}}\begin{pmatrix}2W_{220}^{A}\bar{W}_{131}^{B} + 2W_{311}^{A}\bar{W}_{220}^{B} \\ +4W_{131}^{A}\bar{W}_{040}^{B}\end{pmatrix}$
$W_{333E} = -\frac{1}{\mathcal{K}}(4W_{131}^{A}\bar{W}_{131}^{B} + 4W_{222}^{A}\bar{W}_{222}^{B})$	$W_{511E} = -\frac{1}{\mathcal{K}}\begin{pmatrix}3W_{311}^{A}\bar{W}_{131}^{B} + 8W_{220}^{A}\bar{W}_{040}^{B} \\ +8W_{222}^{A}\bar{W}_{040}^{B}\end{pmatrix}$
$W_{240E} = -\frac{1}{\mathcal{K}}\begin{pmatrix}2W_{131}^{A}\bar{W}_{220}^{B} + 2W_{220}^{A}\bar{W}_{311}^{B} \\ +4W_{040}^{A}\bar{W}_{131}^{B}\end{pmatrix}$	$W_{600E} = -\frac{1}{\mathcal{K}}(4W_{311}^{A}\bar{W}_{040}^{B})$

Pupil distortion figures similar to those of Fig. 1 were taught by Roland Shack in his advanced aberration theory course [3]. The findings that the induced wave aberrations arise from $W_A(\vec{H}, \vec{\rho} + \Delta\vec{\rho}_B)$, and not from $W_B(\vec{H} + \Delta\vec{H}_A, \vec{\rho})$, and their formulas similar to those in Table 2, are due to Hoffman [5]. The compact expression $-\frac{1}{\mathcal{K}}\vec{\nabla}_H\bar{W}_B(\vec{H}, \vec{\rho}) \cdot \vec{\nabla}_\rho W_A(\vec{H}, \vec{\rho})$ for the induced aberrations is due to Sasián [4], [6], and [7]. Sixth-order formulas for the intrinsic wave aberrations, not included here, were developed by Sasián [4], [6] to provide a complete sixth-order theory for axially symmetric systems.

1.3 Theory to Practice

The code to calculate the fourth and sixth order aberration coefficients has been updated to prevent singularities when the marginal ray angle of incidence is zero, or when the marginal ray height is zero. To avoid the singularities the updated code separates the calculation in two parts. One part determines the sixth order coefficients through the formulas in Sasián, and the other part through updated pupil and image aberration relationships [4]. The algorithm is now robust; earlier versions did not quite fix the singularity problems. Several independent tests have been done to check for the correctness of the formulas and macro implementation and they are believed to be correct. For example, when transverse aberrations are calculated from wave aberrations they are found to numerically match those of Buchdahl-Rimmer [8], [9]. One must keep in mind that the sixth order aberration coefficients depend on where the field and aperture vectors are located, as well as where the reference sphere is centered. Buchdahl in his fifth-order treatment chose the object and entrance pupil planes for defining the rays. In wave aberration theory we place the field vector at the object plane, the aperture vector at the exit pupil plane of the system, and the reference sphere is centered at the Gaussian image point.

Crowther and Hoffman have recently written the updated algorithm developed by Sasián [4] into a very capable set of macros for use with CODE V® optical design software. The macros enable not only computation but also plotting and optimization. Any aberration surface contribution to sixth order, intrinsic or induced, or the total aberration sum for a system may be used as operands in an optimization. The macros are now available for download by users of CODE V®.

In the next section, we apply these macros to a design example to demonstrate the computation, plotting, and optimization of lenses using induced and intrinsic sixth order aberration coefficients.

2. DEMONSTRATION OF OPTIMIZATIONS TARGETING SPECIFIC ABERRRATIONS

A useful example for verifying the calculations (used in both [4] and [5]) and the ability to optimize using the calculated aberration coefficients is an aspheric triplet designed by David Shafer [10] to correct all the fourth and sixth order monochromatic aberrations.

2.1 Shafer Triplet

The triplet, shown in Figure 5, is designed at *f*/4.5 with a ± 15° field of view and includes four aspheric surfaces with fourth- and sixth-order coefficients. The original correction used the twelve Buchdahl fifth order ray aberration coefficients, [4], [5]. This system was shown in [4] to provide nearly zero values for the aspheric coefficients at the image using both Sasián's sixth-order theory and Buchdahl's theory, which agrees in the absence of fourth order aberrations.

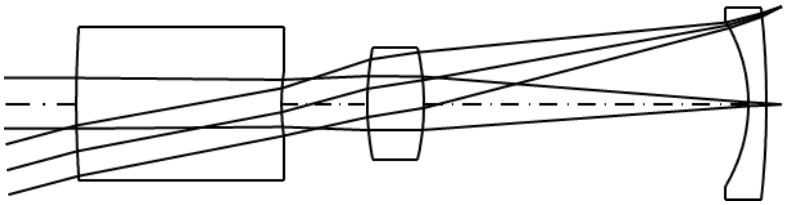

Figure 5. Shafer's aspheric triplet lens corrected for fourth- and sixth-order monochromatic aberrations

To demonstrate optimization using the set of macros developed for calculating and optimizing using constraints on the fourth and sixth order aberration coefficients, we decided to begin with an intentionally rough three-element starting point and use the macros to try to achieve the same goal of correcting all the fourth and sixth order coefficient sums. The initial starting point was a Cooke triplet, which was modified to use Schott N-BK7 glass for all three elements, a wavelength of 587.6 nm, and an effective focal length of 100 mm.

Initially, aspheric surfaces with fourth and sixth order coefficients were used on the same surfaces as the Shafer design (both surfaces on Element 1, and the first surfaces on Elements 2 and 3). However, the starting point was otherwise very different, and did not initially include a field lens element near the image plane. The starting point design is shown in Figure 6. For this study, we have allowed a maximum overall length from the first surface to the image of 200 mm and minimum image clearance of 3 mm.

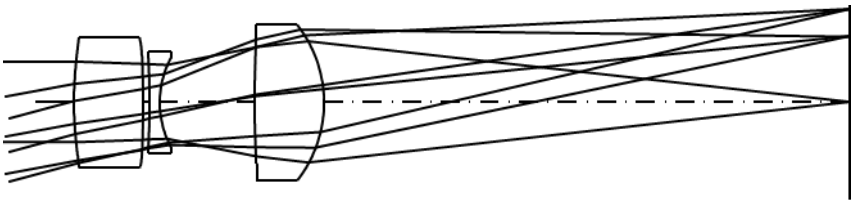

Figure 6. Rough optimization starting point

The system was optimized using weighted constraints on all the fourth order and total (intrinsic plus induced) sixth order aberration coefficient system sums. It was found be very helpful to run a relatively short (< 15 minute) global optimization to allow exploration of the solution space during optimization. It turned out that, when the aspheric coefficients were placed on the same surfaces used in the original triplet design, the form of the best solution closely matched the original design. No other forms of the design were found. The resulting design, which we shall call Design A, is shown in Figure 7. All the fourth and sixth order aberration coefficients were optimized to less than 2×10^{-14} waves. The resulting design looks nearly identical to Figure 5 except for a thicker field lens element.

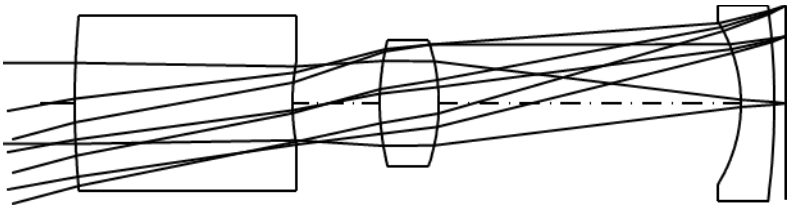

Figure 7. Optimized Design A corrected for fourth and total sixth order aberrations

We also investigated whether placing the four aspheric surfaces on different surface locations could result in other design forms that achieve the goal of correction of all fourth and sixth order aberration coefficients. We found one other design form, in which aspheric surfaces were located on the rear surfaces of Elements 1 and 2, and on both surfaces of Element 3. This solution, which we shall call Design B, was more compact and has a smaller overall RMS wavefront error; all the fourth and sixth order aberration coefficients were optimized to less than 4 x 10^{-14} waves.

Design A, shown in Figure 7, has a composite RMS wavefront error over the field of 0.0499 waves rms, while the new solution, Design B, has a value of 0.0216 waves rms. Design B is shown in Figure 8. The rear element became thicker but the front two elements became much thinner. The overall length from the first lens surface to the image dropped from 196.3 mm to 143.2 mm, and the image clearance increased from 3.0 mm to 14.3 mm. Figure 9 shows the diffraction MTF charts for the two designs. Design B shows a significant improvement at the edge of the field. The lens prescriptions for Design A is given in Table 3, and the prescription for Design B is given in Table 4.

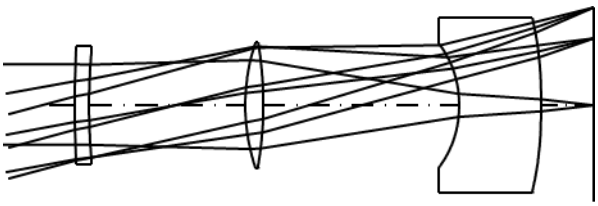

Figure 8. Design B corrected for fourth and total sixth order aberrations

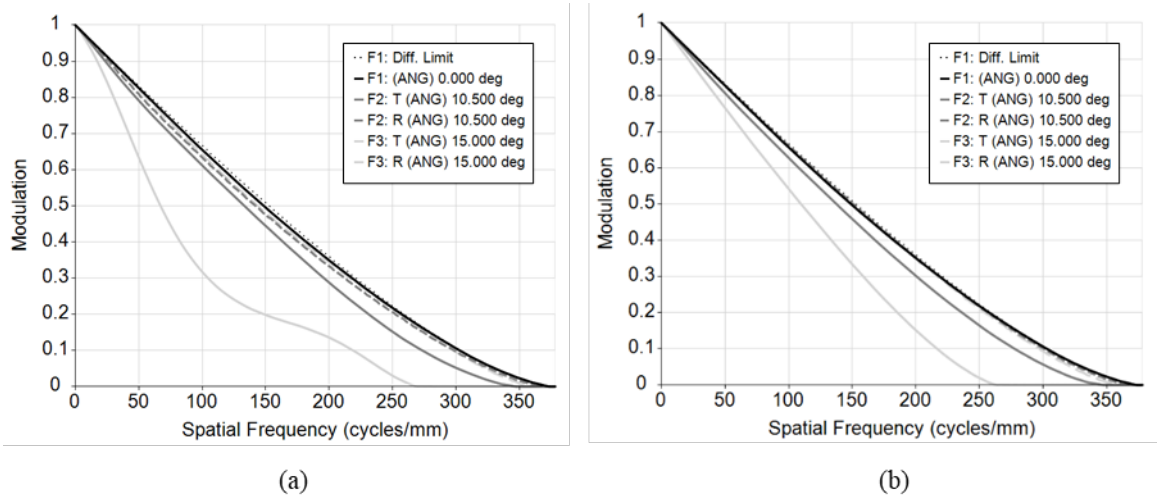

Figure 9. Diffraction MTF as a function of spatial frequency for (a) the original design form and (b) the new design form

Table 3. Constructional Data (mm) of Design A with corrected fourth and total sixth order aberrations[a]

Surface	Radius	Thickness	Glass	A_4	A_6
Object		Infinity			
Entrance pupil		-54.518880			
2	225.788693	60.000000	N-BK7		
3	62.549940	24.292718		-3.914731e-07	-2.780245e-11
4	73.439781	16.137647	N-BK7		
5	-58.434152	83.806061		6.512837e-07	9.674063e-10
6	-41.258247	9.063574	N-BK7	-1.033856e-06	7.809729e-11
7	-197.394165	2.994635		4.690231e-07	-2.564855e-10
Image		0.005365			

[a] The entrance pupil diameter is 22.22222 mm, and the field angle is 15°; λ = 587.6 nm; Effective focal length = 100.000 mm

Table 4. Constructional Data (mm) of Design B with corrected fourth and total sixth order aberrations[a]

Surface	Radius	Thickness	Glass	A_4	A_6
Object		Infinity			
Entrance pupil		-25.260720			
2	650.848396	4.055974	N-BK7		
3	184.924996	42.853189		1.348152e-06	2.533873e-10
4	52.858449	5.288870	N-BK7		
5	-96.469153	53.820235		5.618570e-07	2.463108e-10
6	-31.510562	22.966636	N-BK7	-5.598432e-06	9.653921e-11
7	-158.175959	14.259404		-3.423321e-06	2.172034e-09
Image		-0.005329			

[a] The entrance pupil diameter is 22.22222 mm, and the field angle is 15°; λ = 587.6 nm; Effective focal length = 100.000 mm

As a further aberration visualization aid, it can be useful to plot the aberration coefficients as a function of surface number along with the system aberration sums (Pegel diagrams) for the fourth order and sixth order aberration components (where "S1" indicates the first lens surface). The fourth order aberration coefficient values are shown in Figure 10 for both Designs A and B. Figure 11 shows the intrinsic and induced sixth order aberrations for both designs, and Figure 12 shows the total sixth order aberrations (intrinsic plus induced).

Figure 10 shows that the fourth order coefficient sums are well corrected, and Figure 11 shows that the sixth order intrinsic and induced sums are non-zero but have equal and opposite values to provide a nearly-perfect balance for each total sixth order coefficient.

As shown in Figure 10 and Figure 11, both systems have relatively large surface contributions for fourth order, sixth order intrinsic, and sixth order induced aberrations (in some cases over 100 waves). The distribution of fourth order aberration surface contributions looks similar for many terms, although there are differences in some terms, while the distribution of sixth order aberration surface contributions is much different for the two systems.

The sixth order aberration contributions are more distributed among the surfaces in Design A than Design B. In the new design form, Design B, much of the aberration is coming from the aspheric field lens, particularly for terms with higher field dependence such as W511, W422, W331, and W420. In particular, there is a very large amount of total sixth order distortion, W511, from the first surface of the field lens that is balanced by a large negative W511 term on the rear surface. Design B generally has significantly larger fourth and sixth order aberration surface contributions. Despite that fact, the overall nominal performance of Design B is better than that of Design A.

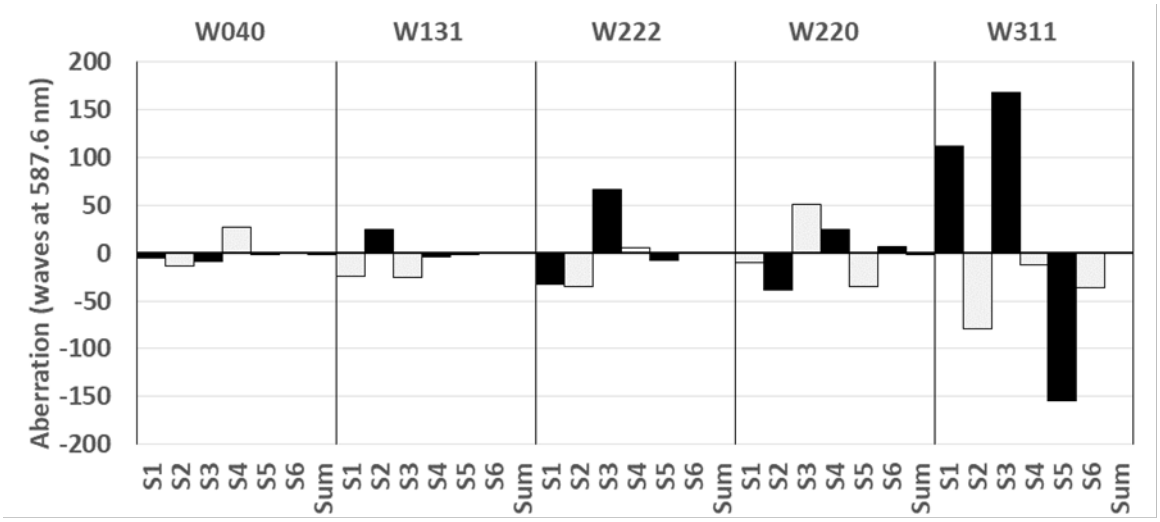

(a)

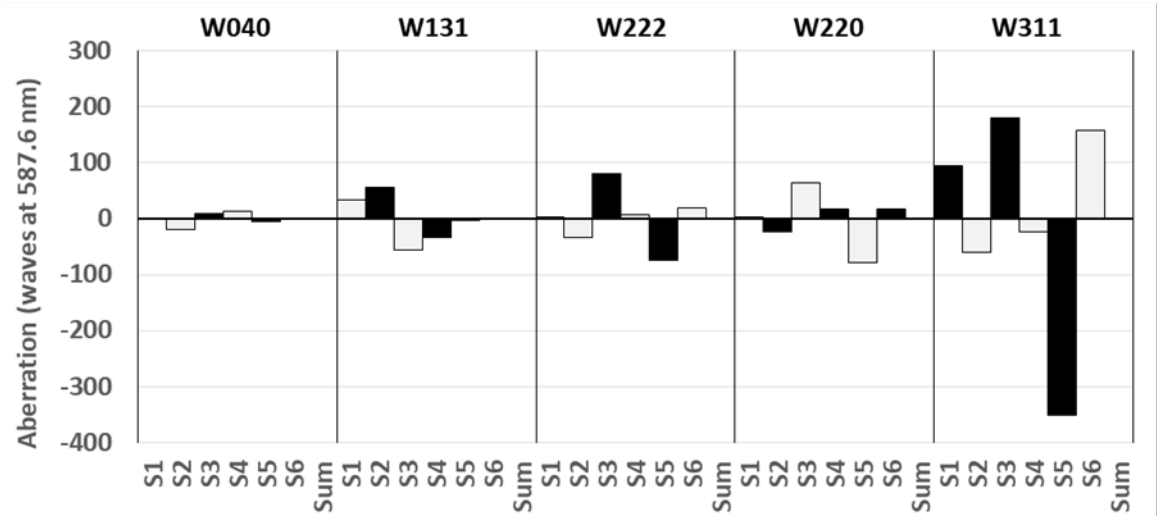

(b)

Figure 10. Fourth order surface contributions and system sums for (a) the original Design A and (b) the new aspheric triplet Design B with corrected fourth order and total sixth order aberration sums.

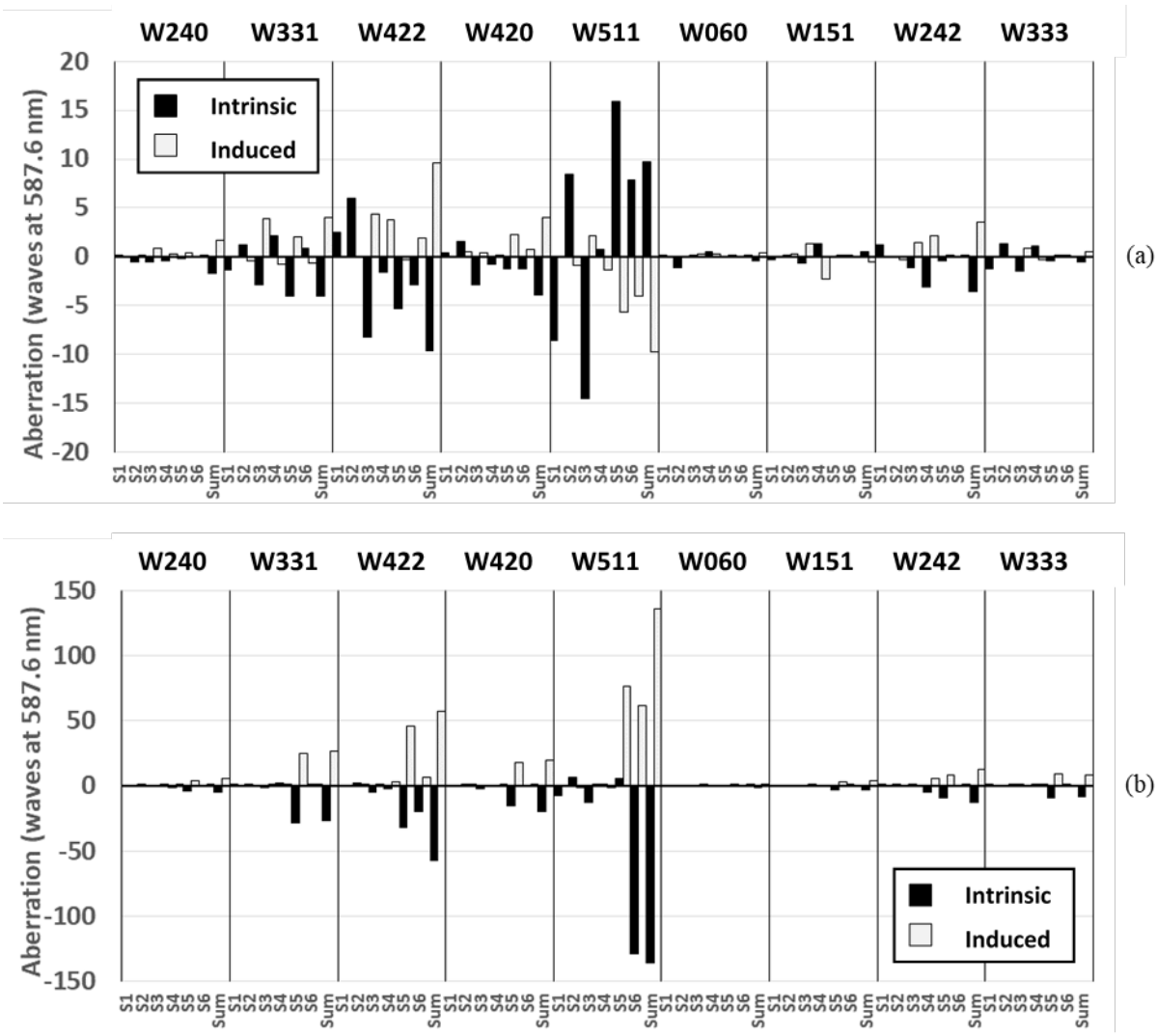

Figure 11. Intrinsic and induced sixth order surface contributions and system sums for (a) the optimized Design A and (b) the new aspheric triplet Design B with corrected fourth order and total sixth order aberrations

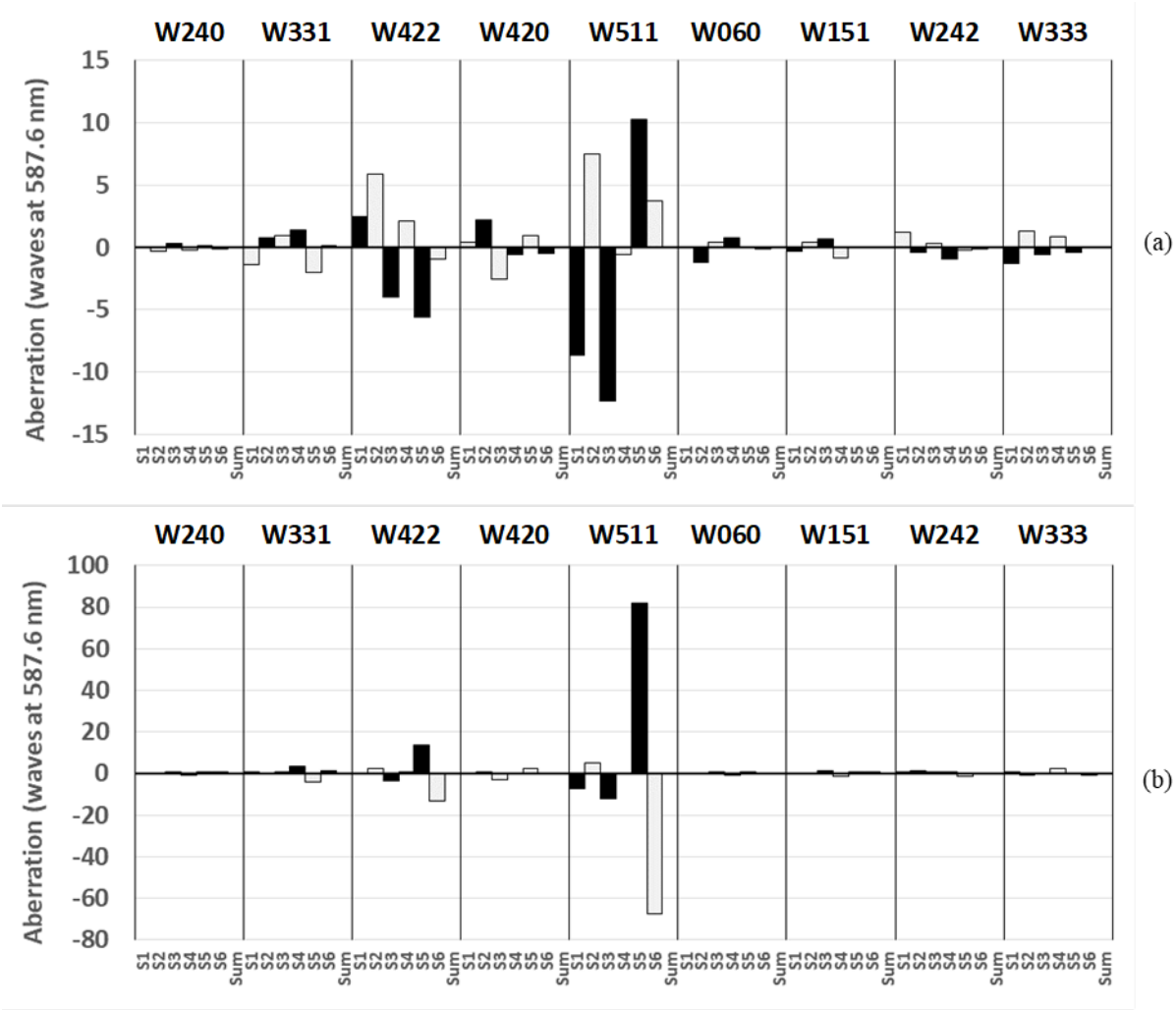

Figure 12. Total sixth order surface contributions and system sums for (a) the optimized Design A and (b) the new aspheric triplet Design B with corrected fourth order and total sixth order aberrations

For Design B, we decided to investigate whether optimization constraints to give an overall reduction in individual surface contributions for sixth order intrinsic and induced aberrations might be useful for driving the design toward a solution that is lens sensitive to manufacturing and alignment tolerances. Instead of constraining the fourth and total sixth order aberration coefficient sums to zero, we applied weighted constraints to reduce the sixth order intrinsic and induced surface contributions and adjusted the weights to minimize the estimated as-built RMS wavefront error.

The resulting design, which we shall call Design C, is shown in Figure 13 and the lens prescription is given in Table 5. By adding constraints to reduce the intrinsic and induced surface contributions, the optimization resulted in a longer, more symmetric system with a front meniscus element and a thick central element. The overall length from the front surface to the image is 177.1 mm, and the image clearance is 3.0 mm. The composite RMS wavefront error is 0.0095 waves, which is slightly improved over Design B. The MTF chart is given in Figure 14; this looks similar to the MTF chart for the starting design, described in Figure 9(b). Figure 15 shows the sixth order intrinsic and induced aberration coefficient surface contributions and system sums, and Figure 16 shows the total sixth order surface contributions. Compared with the starting point Design B, the average coefficient surface contribution magnitude was reduced from 6.0 waves to 0.8 waves. Also, the sixth order aberration surface contributions are much more distributed among the surfaces compared with those of Design B.

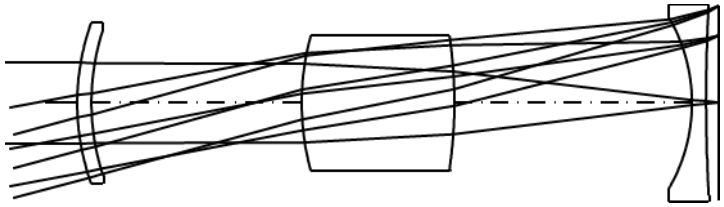

Figure 13. Design C, a reoptimized version of Design B for reduced sixth order intrinsic and induced aberration surface contributions

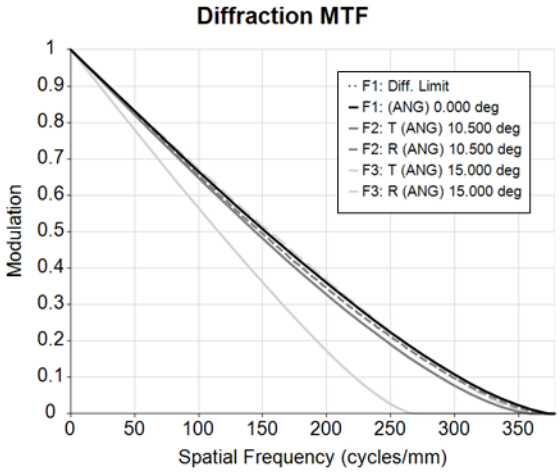

Figure 14. Diffraction MTF as a function of spatial frequency for Design C with reduced sixth order intrinsic and induced surface contributions

Table 5. Constructional Data (mm) of Design C with reduced intrinsic and induced aberrations[a]

Surface	Radius	Thickness	Glass	A_4	A_6
Object		Infinity			
Entrance pupil		-49.453930			
2	66.658571	4.000000	N-BK7		
3	67.352043	57.902070		3.131658e-07	1.425050e-10
4	70.487019	42.268251	N-BK7		
5	-116.567977	65.457863		7.201177e-07	1.082450e-10
6	-48.287061	4.000000	N-BK7	-2.163360e-07	-9.268008e-11
7	522.862381	3.531159		-3.245490e-07	8.975350e-11
Image		-0.017604			

[a] The entrance pupil diameter is 22.22222 mm, and the field angle is 15°; λ = 587.6 nm; Effective focal length = 100.000 mm

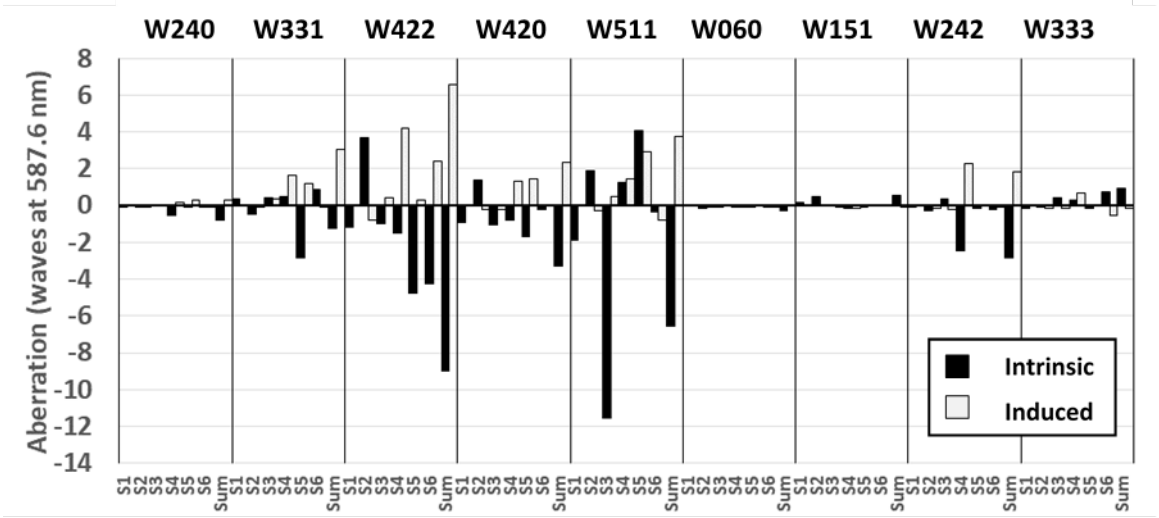

Figure 15. Intrinsic and induced sixth order surface contributions and system sums for Design B2 with reduced sixth order intrinsic and induced surface contributions

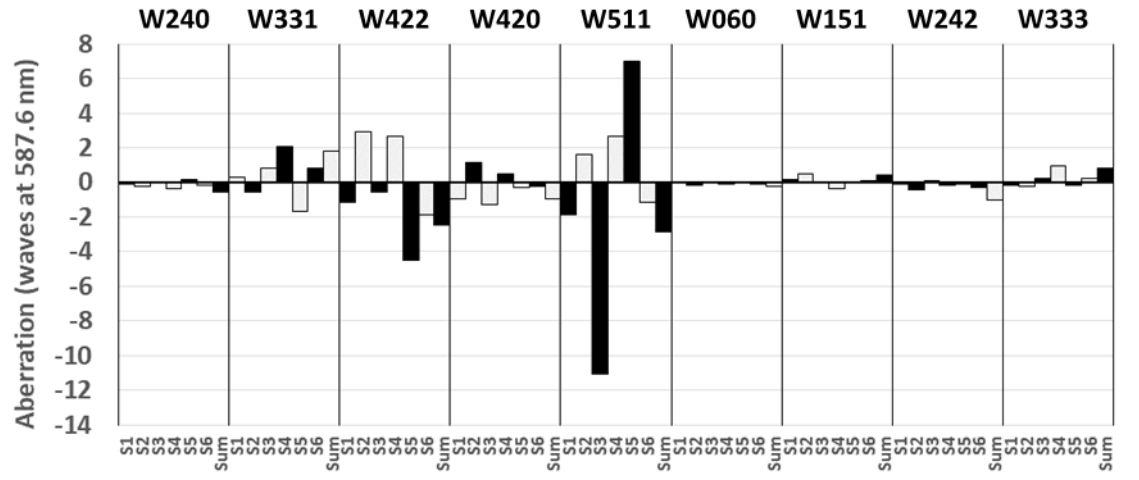

Figure 16. Total sixth order surface contributions and system sums for Design C with reduced sixth order intrinsic and induced surface contributions

To compare the designs, we ran the fast wavefront differential tolerancing option (TOR) in CODE V® using the default set of tolerances (Power: 5 fringes @ 546.1 nm, Irregularity: 1 fringe; Radius of Curvature, Element/Air Thickness, and Element Decenter: 0.025 mm, Wedge: 0.025 mm TIR, Element Tilt: 1 mrad barrel, Index of Refraction: 0.001) and a focus compensator.

The results were evaluated for Design A and Design B, the two design forms with zero fourth and total sixth order aberrations, and Design C, the new design form with reduced intrinsic and induced aberration surface contributions. The resulting performance parameters are listed in Table 6. Design B, with zero fourth and total sixth order coefficients, has better nominal performance than Design A, the original form, but as shown, it has larger sensitivity tolerances. After optimizing for reduced intrinsic and induced surface contributions, the maximum nominal RMS wavefront error dropped from 0.0236 to 0.0118 waves RMS, and the maximum estimated as-built (mean plus 2σ) RMS wavefront error dropped from 0.2674 to 0.0897 waves RMS. Thus, by using weighted constraints for individual sixth order intrinsic and induced aberration surface contributions, we were able to drive the system toward a design with significantly reduced tolerance sensitivity.

Table 6. Nominal and estimated as-built RMS wavefront error (in waves) vs. field for the three aspheric triplet designs using a set of representative tolerances

Aspheric Triplet Design	Object angle (degrees)	RMS WFE, Design	RMS WFE, Est. As-Built	Compensator Range (± in mm)
Design A (zero 4^{th} and total 6^{th} order sums)	0	0.0242	0.0995	0.44
	10.5	0.0386	0.1738	
	15	0.0830	0.2297	
Design B (zero 4^{th} and total 6^{th} order sums)	0	0.0222	0.0959	0.47
	10.5	0.0236	0.2251	
	15	0.0197	0.2674	
Design C (reduced intrinsic/induced surface contributions)	0	0.0071	0.0486	0.23
	10.5	0.0118	0.0800	
	15	0.0111	0.0897	

3. CONCLUSIONS

We have noted that while the total aberrations may be well-corrected at the image plane, lenses typically have significant amounts of both intrinsic and induced aberrations. The formulas for the aberration coefficients demonstrate that the aberration generation behavior is generally very complex. The balance of terms is strongly tied to the first order layout of the system.

Visualizing the surface contributions for the sixth order components through plotting can provide insight into which surfaces contribute more significantly to the system sum for a particular aberration form and type (e.g., intrinsic, induced, or total sixth order). The macros developed for optimization can be used to target individual surface contributions and specific aberration types in order to reduce those contributions or change the aberration balance. The macros can also target system aberration sums by form and type. Because of the complex balance of aberration contributions, using optimization targets for specific aberrations will often force the system into a new design form. This is a tool that can be used in lens optimization.

We have found that targeting aberration contributions can produce designs with reduced tolerance sensitivity. This can result in a higher as-built lens performance. Targeting specific aberrations to achieve the best performance, either as-designed or as-built, requires intuition gained by experience and some trial and error but it can be a useful tool for optimization.

Optimization of a lens using any desired constraints on fourth order or sixth order intrinsic, induced, or total wave aberrations, for individual surfaces or system sums, is a reality. We believe this is something Dr. Shack would have enjoyed seeing, his legacy developed theoretically and commercially to the point that it is a mainstream capability.

REFERENCES

[1] Hopkins, H. H., *The Wave Theory of Aberrations* (Oxford University Press, 1950).
[2] Shack, R. V., "Introduction to Aberrations, Course Notes," University of Arizona, 1993.
[3] Shack, R. V., "Advanced Aberration Theory, Course Notes," University of Arizona, 1993.
[4] Sasián, J., *Introduction to Aberrations in Optical Imaging Systems* (Cambridge University Press, New York, 2013).
[5] Hoffman, J., *Induced Aberrations in Optical Systems*, Ph.D. dissertation (University of Arizona, 1993).
[6] Sasián, J., "Theory of sixth-order wave aberrations," Applied Optics **49**(16), 2010.
[7] Sasián, J., "Extrinsic aberrations in optical imaging systems," Adv Opt Tech **2**(1), 2013.
[8] Buchdahl, H. A., "*Optical Aberrations Coefficients*," (Dover, New York, 1968).
[9] Rimmer, M. P., "Optical aberration coefficients," M.S. thesis (University of Rochester, 1963).
[10] Shafer, D., private communication described in [5], 1992.

ACKNOWLEDGEMENTS

We acknowledge the prior contributions of Ryan Irvin and Weichuan Gao in coding the aberration computations in CODE V macro language.